

# Achieving the performance of the MMSE receiver with the maximum ratio combiner

Diego Fernando Carrera<sup>1\*</sup>, Cesar Vargas-Rosales<sup>2</sup>, Leyre Azpilicueta<sup>2</sup>, Fausto Granda<sup>3</sup>

<sup>1</sup>Research Department, Universidad Tecnológica Empresarial de Guayaquil, Guayaquil 090511, Ecuador

<sup>2</sup>Tecnologico de Monterrey, School of Engineering and Sciences, Monterrey, N.L., Mexico, 64849

<sup>3</sup>Universidad de las Fuerzas Armadas ESPE, Electrical and Electronic Engineering Department, Sangolqui, Ecuador 171-5-231B

\* E-mail: dfcarrera@ieee.org

**Abstract:** In this paper, we study the problem of achieving the wireless performance of the minimum mean square error (MMSE) receiver with the maximum ratio (MR) combiner for massive multiple-input multiple-output (MIMO) systems in the frequency bands of 2.5 GHz and 28 GHz. We propose a new pilot mapping method to jointly estimate the channel state information of the user of interest and reduce the interference effects of multiuser multicell mobile scenarios. By transmitting fewer pilots in the uplink communications, and arranging those pilots to reduce interuser interference, we can achieve higher spectral efficiency (SE) with the MR and MMSE receivers. The achievable SE of the proposed method was studied with the MR combiner and the MMSE receiver. Numerical results show that the combination of the proposed pilot mapping strategy, Kalman filtering estimation, and MR combining results in an SE comparable to that of the MMSE receiver, requiring significantly fewer floating-point operations for MIMO processing.

## 1 Introduction

The growing demand for wireless communications demands a suitable mobile infrastructure capable of addressing higher data rates. This fundamental wireless issue, as a physical layer problem, gives us the need to provide ever-increasing total wireless throughput reliably and uniformly throughout a designated area [1]. The fifth-generation (5G) of mobile communications, commonly known as New Radio (NR), has been developed to fulfill these needs through massive multiple-input multiple-output (MIMO) systems. In the uplink (UL), the MIMO channel hardening property enhances the quality of channel estimation [2]. In the downlink (DL), the beamforming gain enhances the channel capacity since it helps to send out concentrated wireless radiation beams to every user equipment (UE) in the cell. To get the maximum benefits of using massive MIMO systems, the base station (BS) needs to estimate an accurate channel state information (CSI) of the propagation environment to combine the received signal in the reverse link (UL), and precode, the transmitted signal in the forward link (DL) [3].

Coherent wireless systems use reference signals (pilots) to perform channel estimation. Specifically, there is the need to reuse pilots between cells, which wrecks pilot contamination. This effect limits the performance of massive MIMO systems due to intra- and inter-cell interference that cannot be rejected solely with the addition of more antennas at the BS [4]. Another effect that reduces the wireless performance is the thermal noise at the receiver, especially for high path loss scenarios like those in the millimeter-wave (mmWave) band, where the received signal is in a deep fade. Therefore, it is necessary to overcome these effects in the estimation process to get an accurate CSI, rejecting the interference effects, thereby increasing the spectral efficiency (SE) [3].

In the work of [5], the maximum-ratio (MR) combiner is described as an algorithm that maximizes the received signal power, even the interference power, whereas the minimum mean squared error (MMSE) receiver maximizes the signal-to-interference-plus-noise ratio (SINR) at the BS. However, the latter requires a significant amount of complex operations due to the need for matrix inversion operations. On the other hand, the MR combiner requires a few complex operations but compromises the wireless performance in interference-limited scenarios.

According to Sanguinetti *et al.* [6], the MR combiner is a simple MIMO technique that cannot filter out coherent interference, and the MMSE receiver can partially filter the coherent interference, namely, the interference provoked by pilot contamination. This work also shows that the multicell MMSE (M-MMSE) receiver mitigates both intra- and inter-cell interference, resulting in a SE that scales with the number of antennas at the BS. In contrast, MR and MMSE are limited by the pilot contamination effect. However, both techniques require fewer complex operations than the M-MMSE receiver at the cost of lower SE [7]. However, the BS can estimate the CSI of the user of interest, and interferent users that use distinct pilot sequences only when the pilot reuse factor is greater than one, this limits the use of the M-MMSE receiver in high dense multi-cell scenarios [3].

In summary, the M-MMSE receiver has demonstrated to be the optimal combining method in scenarios with coherent and noncoherent interference. However, it is conditioned to get an accurate estimation of the interfering channel at the same time the channel of the user of interest is estimated. Another constraint is that the M-MMSE receiver requires an infeasible amount of complex operations for real-time operation, which limits the practical use of this receiver. Thus, simple linear MIMO techniques like MR and MMSE receivers are a common choice. Therefore, the MIMO processing problem is reduced to minimizing the complexity of the M-MMSE receiver or increasing the performance of the MR and MMSE receivers. In either case, an accurate CSI of the user of interest is required.

Additionally, in this study, we consider the case of mmWave frequencies. According to Akdeniz *et al.* in [8], at mmWave frequencies, the omnidirectional path loss is around 20 to 25 dB higher than the path loss at below 6 GHz (sub6-GHz) frequencies. However, with the reduced wavelength of mmWave signals, the path loss is compensated with the antenna gain that hundreds of antennas in a small array can produce at mmWave frequencies. Furthermore, the high beamforming gain also allows reducing not just the path loss effects, but also the delay and Doppler effects.

In this paper, we introduce a novel pilot mapping strategy to jointly estimate the channel of an intended UE while reducing the interference effects provoked by UEs inside the cell of interest and neighboring cells. This method relies on the mapping of pilots in a quarter of the resource elements (REs) of the orthogonal frequency division multiplexing (OFDM) symbol used for pilot transmission,

and the arrangement of those pilots to reduce the interuser interference. This shift in the pilot transmission between REs allows to obtain an accurate CSI of the desired UE, therefore increasing the SE.

Perfect CSI is not considered at the BS, so the estimation of the CSI of the intended channel was performed with the least-squares (LS) and the Kalman Filter (KF) techniques. Additionally, we consider realistic sub6-GHz and mmWave channels, the effect of limited mmWave scattering and large tightly packed arrays, fully- and partially connected hybrid structures, and a cyclic prefix orthogonal frequency division multiplexing (CP-OFDM) communication based on the Third Generation Partnership Project (3GPP), Release 15 specifications [9]. The contributions of this work are summarized as follows:

- We provide a pilot mapping strategy that allows us to accurately estimate the CSI of the user of interest while reducing coherent and noncoherent interference effects to achieve higher SE.
- For sub6-GHz and mmWave operation frequencies, we tested the performance of MR processing with KF channel estimation when the proposed pilot mapping strategy is used for channel estimation considering frequency-selective channels. Due to the effectiveness of the KF estimation to remove the effects of noise in signals with high path loss, the MR processing achieves the performance of the MMSE receiver, requiring significantly less complex operations.
- Considering fully digital and hybrid beamforming arrays, we provide an analysis of the performance of the MR and MMSE receivers, in terms of the achievable SE and the number of complex operations required when the proposed interfering channel estimation and rejection strategies are used.

The remainder of this work is organized as follows. Section 2 presents the system model and related variables. The proposed pilot mapping and channel estimation methods are outlined in Section 3. In Section 4, the numerical results of the proposed solutions are presented and discussed. Finally, concluding remarks are given in Section 5.

**Notation:** Scalars are denoted in lower case. Bold upper case and lower case denote matrices and vectors, respectively. For any general matrix or vector,  $\mathbf{x}^T$  represents the transpose, and  $\mathbf{x}^H$  the Hermitian transpose. We use  $\text{diag}(x_1, \dots, x_n)$  to represent a diagonal matrix whose diagonal elements are the corresponding components from matrix  $\mathbf{X}$ .  $\mathbf{I}_N$  is an identity matrix of dimension  $N$ , whereas  $\mathbf{1}_N$  is an all-ones vector of dimension  $N$ .  $\|\cdot\|_F$  represents the Frobenius norm operator. The expectation and variance operators are denoted by  $\mathbb{E}[\cdot]$  and  $\mathbb{V}[\cdot]$ , respectively. Finally, a circular symmetric complex Gaussian stochastic vector is written as  $\mathbf{x} \sim \mathcal{CN}(\mu_{\mathbf{x}}, \sigma_{\mathbf{x}}^2)$  with mean  $\mu_{\mathbf{x}}$  and variance  $\sigma_{\mathbf{x}}^2$ .

## 2 System model

We consider a multicell multiuser massive MIMO system with  $L$  cells, where each cell has a BS equipped with  $M$  antennas, and  $K$  randomly located UEs, each equipped with  $N_t$  antennas, as is illustrated in Fig. 1. We assume the BSs share the same band of frequencies and the same set of  $K$  pilot sequences. We assume each cell operates according to the time-division duplexing (TDD) protocol, which is synchronized across the cells.

In Fig. 2, we show a fully digital massive MIMO BS, capable of spatially multiplexing multiple users. A dedicated radio frequency (RF) chain is available for each antenna at the BS, and the  $M$ -antennas are divided into  $R$  subarrays, each comprising  $N_r$  antennas. With this arrangement, the number of UEs that can be spatially multiplexed (simultaneously served) at each BS is upper bounded by  $K \leq R$ . We consider that fully digital beamforming is available only for sub6-GHz frequencies. However, for the mmWave band, we consider hybrid beamforming structures, such as the partially- and fully connected hybrid array structures, as is illustrated in Fig. 3.

Fig. 3 shows the block diagram of a mmWave BS for partially and fully connected hybrid beamforming structures, considering the UL

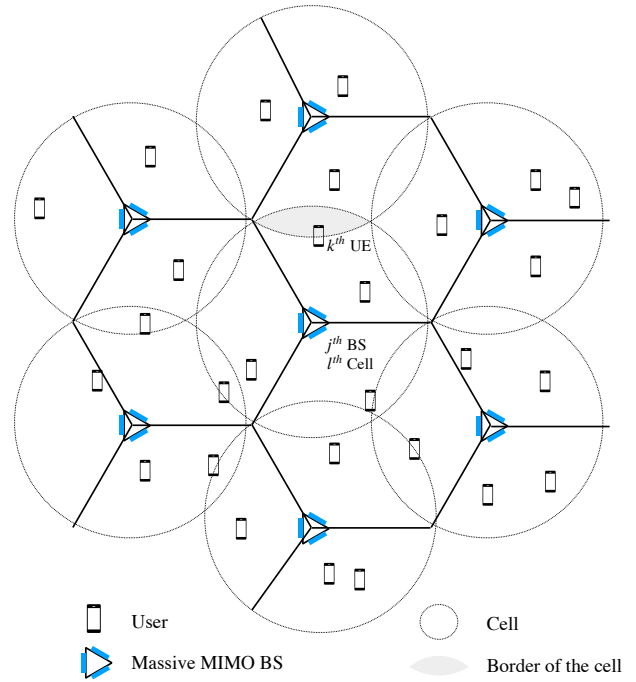


Fig. 1: Multi-user multi-cell massive MIMO scenario.

and DL processing. In hybrid array structures, there are fewer RF chains than antennas at the BS since MIMO combining and precoding processing is divided into analog and digital domains. Therefore, the number of RF chains available for a hybrid structure is  $R < M$ . For a partially connected hybrid array structure, each RF chain is mapped to a subarray of  $N_r$  antennas through analog RF precoders (phase shifters and gain control units); hence, there are  $RN_r = M$  phase shifters. For a fully connected hybrid array structure, each analog RF precoder is mapped to  $M$  antennas at the BS. Thus, this structure requires  $RM$  phase shifters [10, 11]. According to Ahmed *et al.* [12], the beamforming gain for the fully-connected structure is  $R \log(R)$  higher in terms of the SE than the partially-connected structure, with  $R$  times more power consumption.

The block diagram on the left-hand side of Fig. 3, shows the hybrid array structure for the UL communication, where the  $M$  antennas at the BS are divided into  $R$  subarrays of  $N_r$  receiving antennas where MIMO combining is performed. The block diagram on the right-hand side of Fig. 3 shows the hybrid array structure for the DL communication. In this case, the  $M$  antennas at the BS are divided into  $R$  subarrays of  $N_t$  transmitting antennas where MIMO precoding processing is performed.

### 2.1 Uplink training

$K$  UEs in each cell independently transmit data signals to their respective BS. However, those signals can be received at the BSs in neighboring cells. As is illustrated in Fig. 2, the transmitted signal from user  $k$  in cell  $l$  to the BS  $j$ , is given by  $\phi_{jlk}[s] = \mathbf{f}_{jlk}[s]s_{jlk}$ , where  $s_{jlk}$  represents the subcarrier data symbol for  $s = 1, \dots, S$ . We assume the data symbols transmitted by each UE are statistically independent. On the other hand, we assume the transmitted  $k^{\text{th}}$  UE data symbol is precoded, therefore  $\mathbf{f}_{jlk}[s]$  represents the  $N_t \times 1$  precoding vector. Precoding for the sub6-GHz band is assumed to be fully digital, whereas, for the mmWave band, we assume hybrid precoding is required.

The precoding vector  $\mathbf{f}_{jlk}[s]$  is equivalent to

$$\mathbf{f}_{jlk}[s] = \begin{cases} \mathbf{f}_{\text{BB}jlk}[s], & \text{for the sub6-GHz band} \\ \mathbf{F}_{\text{RF}jl}^r \mathbf{f}_{\text{BB}jlk}[s], & \text{for the mmWave band,} \end{cases} \quad (1)$$

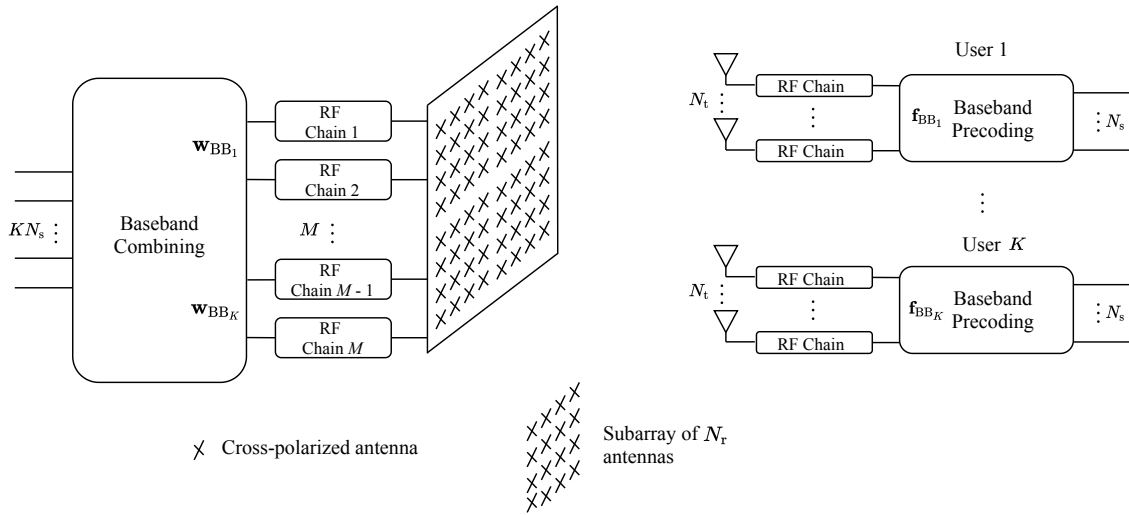


**Fig. 2:** Simplified block diagram of a multi-user massive MIMO system. The BS performs spatial multiplexing to serve simultaneously  $K$  users.

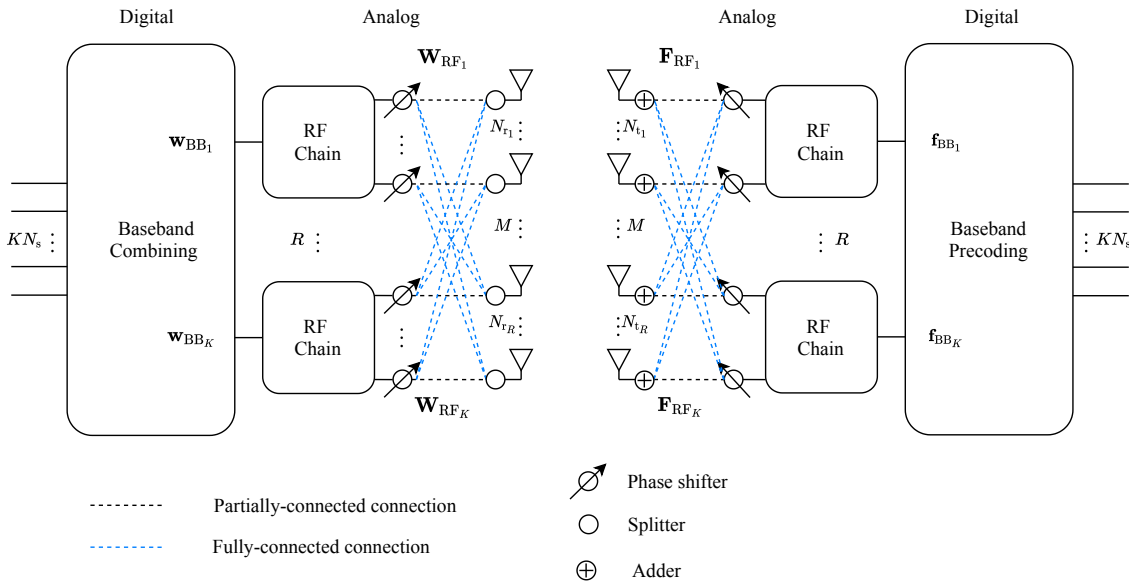


**Fig. 3:** Simplified block diagram of a multi-user mmWave system for partially and fully-connected hybrid array structures.

where  $\mathbf{f}_{BB_{jl}k}[s]$  denotes the  $N_t \times 1$  fully-digital baseband (BB) precoder, and  $\mathbf{F}_{RF_{jl}^r}$  is the  $N_t \times N_t$  matrix of the RF analog precoder at the  $r^{th}$  subarray of the  $j^{th}$  BS in the  $l^{th}$  cell [13].

Given that there are  $K$  users per cell, throughout the paper, we use the subscript  $i$  instead of  $k$ , for  $i = 1, 2, \dots, K$ , to denote the user of interest, and its corresponding precoding vector and channel matrix. Additionally, we consider cell  $j$  as the cell of interest. Accordingly, the  $s^{th}$  subcarrier received signal  $\mathbf{y}_{jj}^r[s]$  at the  $r^{th}$  subarray of the  $j^{th}$  BS in cell  $j$ , represented as a  $N_r \times 1$  vector, is given by

$$\begin{aligned} \mathbf{y}_{jj}^r[s] = & \underbrace{\sqrt{\rho_{ji}} \mathbf{H}_{jji}^r[s] \mathbf{f}_{jji}[s] s_{jji}}_{\text{desired signal}} \\ & + \underbrace{\sum_{k=1, k \neq i}^K \sqrt{\rho_{jk}} \mathbf{H}_{jjk}^r[s] \mathbf{f}_{jjk}[s] s_{jjk}}_{\text{intra-cell interference}} \\ & + \underbrace{\sum_{l=1, l \neq j}^L \sum_{k=1}^K \sqrt{\rho_{lk}} \mathbf{H}_{ljk}^r[s] \mathbf{f}_{ljk}[s] s_{ljk} + \mathbf{n}_{jj}^r[s]}_{\text{inter-cell interference plus noise}}, \quad (2) \end{aligned}$$

where  $\mathbf{H}_{jji}^r[s]$  and  $\mathbf{H}_{jjk}^r[s]$  are the  $N_r \times N_t$  channel matrices between the  $r^{th}$  subarray of the  $j^{th}$  BS, and the  $i^{th}$  and  $k^{th}$  UEs in cell  $j$ , respectively, whereas  $\mathbf{H}_{ljk}^r[s]$  is the  $N_r \times N_t$  channel matrix between the  $k^{th}$  UE in the  $l^{th}$  neighbor cell and the  $r^{th}$  subarray of the  $j^{th}$  BS in cell  $j$ .  $\rho_{ji}$  and  $\rho_{jk}$  denote the transmission power of the  $i^{th}$  and  $k^{th}$  UEs in cell  $j$ , respectively, whereas  $\rho_{lk}$  denotes the

transmission power of the  $k^{th}$  UE in the  $l^{th}$  cell.  $\mathbf{n}_{jj}^r[s]$  is the  $N_r \times 1$  vector characterized as i.i.d.  $CN(0, \sigma_{jr}^2)$  noise at the  $r^{th}$  subarray of the  $j^{th}$  BS in cell  $j$ . Assuming orthogonal pilots are used for UL training with the  $K$  spatially multiplexed UEs at the  $j^{th}$  BS in cell  $j$ , the intra-cell interference becomes non-coherent interference. On the other hand, assuming a cell frequency reuse factor  $f = 1$ , pilot sequences used by UEs in neighbor cells provoke coherent interference to the UL training of the  $j^{th}$  BS in cell  $j$  [6, 13–15].

Nevertheless, the received signal  $\mathbf{y}_{jj}^r[s]$  in (2) is only true for fully-digital massive MIMO BSs, for  $\mathbf{f}_{jlk}[s] = \mathbf{f}_{BB,jlk}[s]$ . At mmWave frequencies, considering a hybrid beamforming structure, the received signal  $\mathbf{y}_{jj}^r[s]$  at the  $r^{th}$  subarray of the  $j^{th}$  BS in cell  $j$  is given by  $\mathbf{W}_{RF,jj}^r \mathbf{y}_{jj}^r[s]$ , where  $\mathbf{W}_{RF,jj}^r$  is the  $N_r \times N_r$  matrix of the RF combiner at the  $r^{th}$  subarray of the  $j^{th}$  BS in cell  $j$  [13].

Each BS uses the estimated CSI of the  $i^{th}$  UE to perform MIMO combining and precoding. The combining operation for fully digital massive MIMO systems is written as

$$\begin{aligned} \hat{s}_{jji} &= \mathbf{w}_{jji}^H[s] \mathbf{y}_{jj}^r[s] \\ &= \sqrt{\rho_{ji}} \mathbf{w}_{jji}^H[s] \mathbf{H}_{jji}^r[s] \mathbf{f}_{jji}[s] s_{jji} \\ &\quad + \sum_{k=1, k \neq i}^K \sqrt{\rho_{jk}} \mathbf{w}_{jji}^H[s] \mathbf{H}_{jjk}^r[s] \mathbf{f}_{jjk}[s] s_{jjk} \\ &\quad + \sum_{l=1, l \neq j}^L \sum_{k=1}^K \sqrt{\rho_{lk}} \mathbf{w}_{jji}^H[s] \mathbf{H}_{jlk}^r[s] \mathbf{f}_{jlk}[s] s_{jlk} \\ &\quad + \mathbf{w}_{jji}^H[s] \mathbf{n}_{jj}^r[s], \end{aligned} \quad (3)$$

where  $\hat{s}_{jji}$  is the combined symbol, transmitted by the  $i^{th}$  UE at the  $j^{th}$  BS in cell  $j$ , and  $\mathbf{w}_{jji}[s]$  is the corresponding  $N_r \times 1$  combining vector. The combining operation is considered as fully-digital for the sub6-GHz band and hybrid for the mmWave band. For the mmWave band, the combining operation is given by

$$\begin{aligned} \hat{s}_{jji} &= \mathbf{w}_{jji}^H[s] \mathbf{W}_{RF,jj}^r \mathbf{y}_{jj}^r[s] \\ &= \sqrt{\rho_{ji}} \mathbf{w}_{jji}^H[s] \mathbf{W}_{RF,jj}^r \mathbf{H}_{jji}^r[s] \mathbf{f}_{jji}[s] s_{jji} \\ &\quad + \sum_{k=1, k \neq i}^K \sqrt{\rho_{jk}} \mathbf{w}_{jji}^H[s] \mathbf{W}_{RF,jj}^r \mathbf{H}_{jjk}^r[s] \mathbf{f}_{jjk}[s] s_{jjk} \\ &\quad + \sum_{l=1, l \neq j}^L \sum_{k=1}^K \sqrt{\rho_{lk}} \mathbf{w}_{jji}^H[s] \mathbf{W}_{RF,jj}^r \mathbf{H}_{jlk}^r[s] \mathbf{f}_{jlk}[s] s_{jlk} \\ &\quad + \mathbf{w}_{jji}^H[s] \mathbf{W}_{RF,jj}^r \mathbf{n}_{jj}^r[s]. \end{aligned} \quad (4)$$

Hence,  $\mathbf{w}_{jji}[s]$  is equivalent to

$$\mathbf{w}_{jji}[s] = \begin{cases} \mathbf{w}_{BB,jji}[s], & \text{for the sub6-GHz band} \\ \mathbf{W}_{RF,jj}^r \mathbf{w}_{BB,jji}[s], & \text{for the mmWave band,} \end{cases} \quad (5)$$

where  $\mathbf{w}_{BB,jji}[s]$  denotes the  $N_r \times 1$  digital BB combiner [13, 16–18].

With the  $N_r \times 1$  estimated channel vector of the  $i^{th}$  UE,  $\hat{\mathbf{h}}_{jji}[s]$ , to be described in Section 3.2, common linear MIMO processing techniques, such as the MR and MMSE receivers, are used to find the BB combining vector, which is given by

$$\mathbf{w}_{BB,jji}[s] = \begin{cases} \hat{\mathbf{h}}_{jji}[s] / \|\hat{\mathbf{h}}_{jji}[s]\|_F^2 & \text{MR} \\ \left[ \hat{\mathbf{H}}_i^H \hat{\mathbf{H}}_i + \sigma_{jr}^2 \mathbf{I}_{N_r} \right]^{-1} \hat{\mathbf{h}}_{jji}[s] & \text{MMSE,} \end{cases} \quad (6)$$

where  $\hat{\mathbf{H}}_i = [\hat{\mathbf{h}}_{jji}[s], \dots, \hat{\mathbf{h}}_{jji}[s], \dots, \hat{\mathbf{h}}_{jji}[s]]^T$  is the  $K \times N_r$  channel matrix composed of the estimated channels of the  $i^{th}$  users of interest in cell  $j$ . However, the combining operation in (6) is valid only for fully-digital beamforming. For the case of hybrid beamforming, channel estimation, and therefore MIMO combining must be performed on the digital BB received signal  $\mathbf{y}_{BB,jj}^r[s]$ . Thus, the RF combining matrix must be filtered out from  $\mathbf{y}_{jj}^r[s]$ , to do so, the operation is given by

$$\mathbf{y}_{BB,jj}^r[s] = \left[ \mathbf{W}_{RF,jj}^r \mathbf{W}_{RF,jj}^r \right]^{-1} \mathbf{W}_{RF,jj}^r \mathbf{y}_{jj}^r[s]. \quad (7)$$

When the perfect CSI of the  $i^{th}$  UE is used to find  $\mathbf{w}_{jji}[s]$ , and considering fully digital beamforming, the product  $\sqrt{\rho_{ji}} \mathbf{w}_{jji}^H[s] \mathbf{H}_{jji}^r[s] \mathbf{f}_{jji}[s]$  in (3) is equal to the unity gain. Assuming that  $\mathbf{w}_{jji}^H[s] \mathbf{n}_{jj}^r[s] \approx 0$ , we provide the following remark.

**Remark 1:** The combiner output  $s'_{jji}$ , processed with the perfect CSI of the  $i^{th}$  UE, results in

$$\begin{aligned} s'_{jji} &= s_{jji} + \sum_{k=1, k \neq i}^K \sqrt{\rho_{jk}} \mathbf{w}_{jji}^H[s] \mathbf{H}_{jjk}^r[s] \mathbf{f}_{jjk}[s] s_{jjk} \\ &\quad + \sum_{l=1, l \neq j}^L \sum_{k=1}^K \sqrt{\rho_{lk}} \mathbf{w}_{jji}^H[s] \mathbf{H}_{jlk}^r[s] \mathbf{f}_{jlk}[s] s_{jlk} \end{aligned} \quad (8)$$

Note that even performing MIMO combining processing with the perfect CSI of the  $i$  UE, intra- and inter-cell interferences are still present [4, 14, 19]. One option to filter out the interference effects, at least the coherent interference, is to perform interference rejection combining, which requires an accurate channel estimation of the interfering channel, which, in a well-designed network, is small [4, 6]. We propose to reduce the interference effects with a pilot strategy that reduces the number of transmitted pilots and arranges the pilot mapping to reduce the interuser interference, which is introduced in Section 3.

Finally, to perform DL precoding, the signal to be transmitted from the  $j^{th}$  BS to the user  $i$  in cell  $j$  must be processed with the  $N_t \times 1$  precoding vector  $\mathbf{f}_{BB,jji}$ , which is given by

$$\mathbf{f}_{BB,jji}[s] = \frac{\mathbf{w}_{BB,jji}[s]}{\|\mathbf{w}_{BB,jji}[s]\|}, \quad (9)$$

and for mmWave systems, the BB precoding vector is multiplied by the RF precoder, such as  $\mathbf{F}_{RF,jj}^r \mathbf{f}_{BB,jji}[s]$ . It is worth noticing that throughout the paper,  $\mathbf{F}_{RF,jj}^r$  and  $\mathbf{W}_{RF,jj}^r$  are assumed to be codebook matrices.

## 2.2 Channel model

For simplicity, we avoid the use of the subscripts and superscript defined for the channel matrices  $\mathbf{H}_{jji}^r[s]$ ,  $\mathbf{H}_{jjk}^r[s]$ , and  $\mathbf{H}_{jlk}^r[s]$ , so that, in this section, we describe a general MIMO channel model.

Using the clustered channel model in [8, 13], the  $d^{th}$  delay tap of discrete-time narrowband  $N_r \times N_t$  matrix channel  $\mathbf{H}_d$ ,  $d = 0, 1, \dots, N_{c-1}$ , is written as

$$\mathbf{H}_d = \sqrt{\frac{N_r N_t}{N_{cl} N_{ray}}} \sum_{\eta=1}^{N_{cl}} \sum_{\iota=1}^{N_{ray}} g_{\eta\iota} \mathbf{a}_r(\theta_{\eta\iota}^r, \phi_{\eta\iota}^r) \mathbf{a}_t^H(\theta_{\eta\iota}^t, \phi_{\eta\iota}^t), \quad (10)$$

where  $N_c$  denotes the delay tap length in the discrete-time domain,  $g_{\eta\iota}$  is the complex small-scale fading gain of the  $\iota^{th}$  ray in the  $\eta^{th}$  scattering cluster, characterized as i.i.d.  $CN(0, \sigma_{\eta}^2)$ ,  $\sigma_{\eta}^2$  denotes the average power of the  $\eta^{th}$  cluster.  $N_{cl}$  is the number of scattering clusters, whereas  $N_{ray}$  is the number of rays (subpaths). The vectors  $\mathbf{a}_r(\theta_{\eta\iota}^r, \phi_{\eta\iota}^r)$  and  $\mathbf{a}_t^H(\theta_{\eta\iota}^t, \phi_{\eta\iota}^t)$  denote the array response

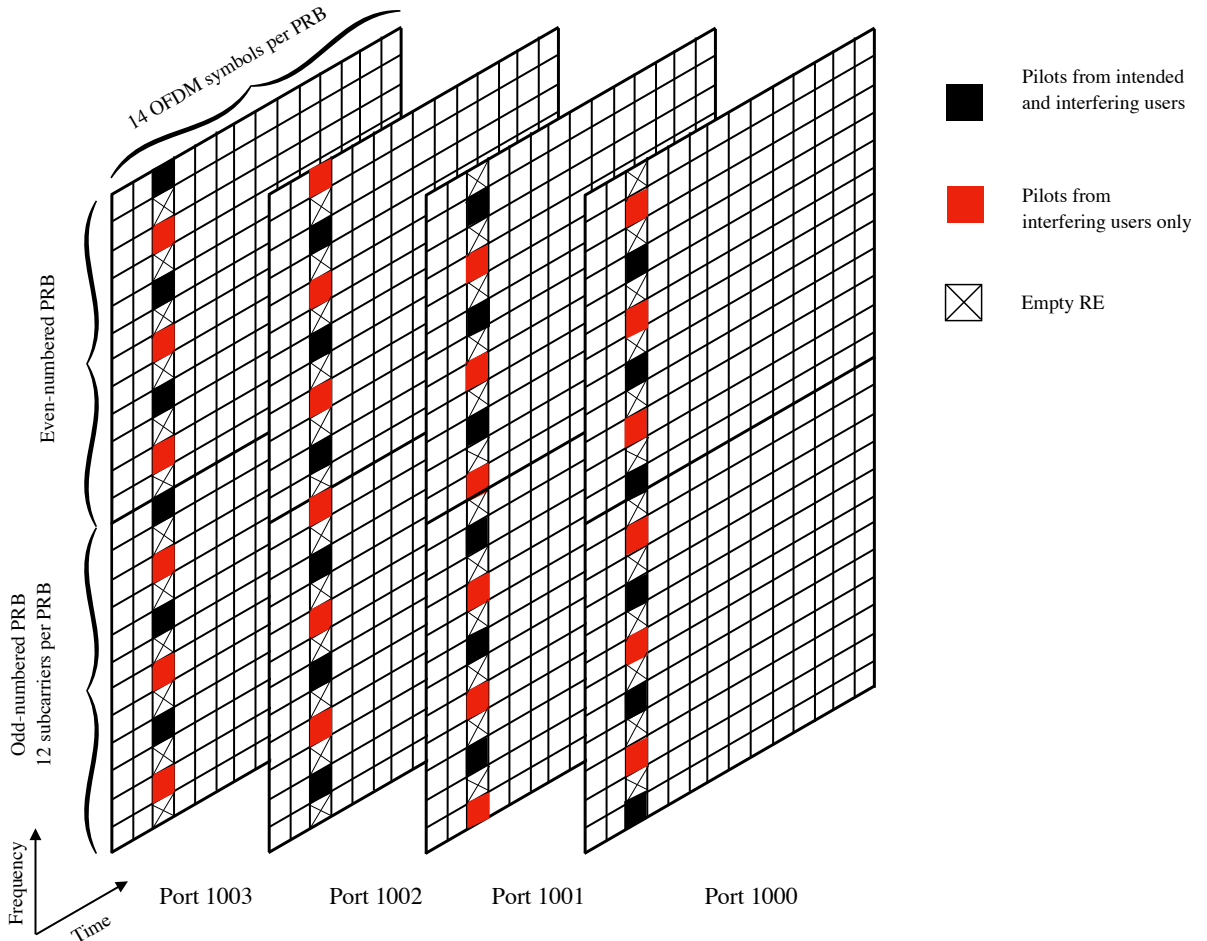


**Fig. 4:** Proposed multi-user dual pilot mapping method. The spatially multiplexed users transmit pilots only in a quarter of the subcarriers of the third OFDM symbol used for pilot mapping. With the proposed pilot locations, the effects of interference are reduced among the different antennas ports.

functions, for the receive and transmit antenna arrays, to the angles of arrival  $\phi_{\eta\iota}^r(\theta_{\eta\iota}^r)$  and departure  $\phi_{\eta\iota}^t(\theta_{\eta\iota}^t)$ , respectively.

To represent the spatial correlation of the channel between the transmitter and receiver, we use the Kronecker model. For sub6-GHz and mmWave frequencies, and assuming Rayleigh fading, the MIMO channel  $\mathbf{H}_d$  is given by

$$\mathbf{H}_d = \mathbf{R}_r^{1/2} \mathbf{G}_d (\mathbf{R}_t^{1/2})^T \quad (11)$$

where  $\mathbf{R}_r = \mathbb{E}[\mathbf{H}_d \mathbf{H}_d^H]$  and  $\mathbf{R}_t = \mathbb{E}[(\mathbf{H}_d^H \mathbf{H}_d)^T]$  are the transmit and receive correlation matrices, and  $\mathbf{G}_d$  is a stochastic  $N_r \times N_t$  matrix with i.i.d.  $\mathcal{CN}(0, 1)$  elements [20].

Finally, as in [21], the frequency-selective channel at subcarrier  $s$ , for  $s = 1, \dots, S$ , in terms of the different time delay taps is given by

$$\mathbf{H}[s] = \sum_{d=0}^{N_c-1} \mathbf{H}_d e^{-j \frac{2\pi s}{S} d}. \quad (12)$$

### 3 Methodology

In this section, we present a novel pilot mapping method to jointly estimate the channel of the user of interest and reduce the interference effects produced by users in the cell of interest and neighbor cells.

#### 3.1 Pilot Mapping

To perform accurate channel estimation, reducing the interference effects, we propose to set the transmission of pilots in the  $i^{th}$  UE only to a quarter of the REs of the OFDM symbol used for pilot transmission, and the arrangement of those pilots to reduce the interuser interference. This way, the interference between the spatially multiplexed UEs reduces. Fig. 4 shows the proposed pilot mapping method, where the pilot sequences in the third and fourth OFDM symbols in the physical resource blocks (PRBs) are mutually orthogonal.

In Fig. 4, the intra-cell interference for up to four UE is significantly reduced since the location of the pilots provokes no interference. Furthermore, to multiplex eight users, the proposed pilot mapping strategy must be repeated, and the four new users must use orthogonal pilots regarding the pilots of the first four ones. With quadrature phase-shift keying (QPSK) modulation, up to four orthogonal pilot sequences can be used. Thus, the proposed pilot mapping structure can be repeated up to four times, allowing the multiplexing of up to 16 users.

With spatial multiplexing, the intracell interference increases, given that orthogonal pilots are used between the multiple users in the cell of interest, which conforms the noncoherent interference. On the other hand, users in neighbor cells can reuse the pilot sequences used by the users of the cell of interest, which provokes coherent interference, commonly known as pilot contamination [6]. However, with the pilot mapping of Fig. 4, the intra- and inter-cell interference can be accurately estimated over the REs not used for pilot transmission.

**Table 1** Fully-digital beamforming simulation parameters

Parameter	Value
Channel model	3GPP 3D MIMO urban-macrocell NLoS
BS array configuration	8 × 8 array with cross polarization (64T64R, $M = 64$ )
UE array configuration	Dual-antenna UEs
Cell radius	500 m
Carrier frequency	2.57 GHz
Carrier type	CP-OFDM (30 kHz of subcarrier spacing)
Carrier bandwidth	40 MHz
NR data slot	12 subcarriers per PRB, 14 OFDM symbols per slot, 102 PRBs in the frequency domain
Occupied subcarriers	1224 subcarriers per OFDM symbol
Channel estimation	LS, KF
Combining processing	MR, MMSE

### 3.2 Channel estimation

During the UL pilot training, to estimate the channels of the  $i^{\text{th}}$  UE, the  $K$  UEs in each cell are assumed to transmit mutually orthogonal pilot sequences. For the UEs in neighboring cells, we assume the reuse of the pilot sequences from the UEs in cell  $j$  [6, 7].

Given the introduced pilot mapping strategy, the channel estimation process for the  $i^{\text{th}}$  UE must be performed over the REs used for pilot transmission. To do so, we define the received signal with pilots from the  $i^{\text{th}}$  UE, represented as a  $N_r \times N_p$  matrix and is given by

$$\begin{aligned}
 \mathbf{y}_{jji}^r[s] = & \underbrace{\sqrt{\rho_{ji}} \mathbf{H}_{jji}^r[s] \mathbf{f}_{jji}[s] x_{jji}}_{\text{desired pilots}} \\
 & + \underbrace{\sum_{k=1, k \neq i}^K \sqrt{\rho_{jk}} \mathbf{H}_{jjk}^r[s] \mathbf{f}_{jjk}[s] x_{jjk}}_{\text{intra-cell pilots}} \\
 & + \underbrace{\sum_{l=1, l \neq j}^L \sum_{k=1}^K \sqrt{\rho_{lk}} \mathbf{H}_{ljk}^r[s] \mathbf{f}_{ljk}[s] x_{ljk}}_{\text{inter-cell pilots}} + \underbrace{\mathbf{n}_{jji}^r[s]}_{\text{noise}}, \quad (13)
 \end{aligned}$$

where  $x_{jji}$ ,  $x_{jjk}$ ,  $x_{jlk}$  are the pilots of the  $i^{\text{th}}$  UE (desired pilots), the  $k^{\text{th}}$  UE in cell  $j$ , and the  $k^{\text{th}}$  UE in the  $l^{\text{th}}$  cell, respectively.  $\mathbf{n}_{jji}^r$  is the  $N_r \times 1$  noise matrix.  $x_{jji}$  is assumed to be orthogonal to  $x_{jjk}$ . However,  $x_{jlk}$  is assumed to reuse the pilot sequence in  $x_{jji}$ , which provokes pilot contamination.

Channel estimation for the  $i^{\text{th}}$  UE with the LS technique is straightforward and is given by

$$\hat{\mathbf{h}}_{jji}[s] = \mathbf{y}_{jji}^r[s] x_{jji}^{-1}. \quad (14)$$

For hybrid beamforming, as in (7), channel estimation in (14) must be performed with the BB received signal with pilots from the  $i^{\text{th}}$  UE, which is written as

$$\mathbf{y}_{\text{BB}jji}^r[s] = \left[ \mathbf{W}_{\text{RF}jj}^r (\mathbf{W}_{\text{RF}jj}^r)^H \right]^{-1} \mathbf{W}_{\text{RF}jj}^r \mathbf{y}_{jji}^r[s]. \quad (15)$$

With the estimated channel of the  $i^{\text{th}}$  UE,  $\hat{\mathbf{h}}_{jji}[s]$ , MIMO combining processing can be performed with the MR and MMSE receivers as in (6). However, the MR combiner cannot achieve the wireless performance of the MMSE receiver only with the decrease of the interference effects. It is necessary to use a better channel estimation technique to reduce noise effects, especially for mmWave signals.

Better channel estimation of the user of interest might increase the performance of MIMO processing. In [22] the KF is presented as a technique capable of reducing the effects of Gaussian noise over

the estimated channel. Furthermore, the performance of KF estimation with MR processing is presented as similar to that of the MMSE receiver when the interference power is small. Hence, with the proposed pilot mapping, we propose to use the KF algorithm with MR processing to achieve the performance of the MMSE receiver, reducing the number of complex operations required for MIMO processing.

The KF estimation can be performed as follows. First, the LS estimation of the initial subcarrier,  $\hat{\mathbf{h}}_{jji}[1] = \mathbf{y}_{jji}^r[1] (x_{jji}[1])^{-1}$ , and its corresponding variance  $\sigma_{\hat{\mathbf{h}}_{jji}}[1] = \mathbb{V}\{\hat{\mathbf{h}}_{jji}[1]\}$  are required to initialize the KF algorithm. The  $s^{\text{th}}$  subcarrier Kalman gain  $\kappa_{jji}[s]$ , for  $s \neq 1$ , is given by

$$\begin{aligned}
 \kappa_{jji}[s] = & \sigma_{\hat{\mathbf{h}}_{jji}}[s-1] x_{jji}[s]^H \\
 & \left( x_{jji}[s] \sigma_{\hat{\mathbf{h}}_{jji}}[s-1] x_{jji}[s]^H + \sigma_{jr}^2 \right)^{-1}. \quad (16)
 \end{aligned}$$

With  $\kappa_{jji}[s]$ , a correction process to the estimated channel at the  $s^{\text{th}}$  subcarrier is required. To do so, the received vector  $\mathbf{y}_{jji}^r[s]$  at the  $s^{\text{th}}$  subcarrier, for  $s \neq 1$ , is used. The correction process is written as

$$\begin{aligned}
 \hat{\mathbf{h}}_{jji}[s] = & \hat{\mathbf{h}}_{jji}[s-1] + \kappa_{jji}[s] \\
 & (\mathbf{y}_{jji}^r[s] - x_{jji}[s] \hat{\mathbf{h}}_{jji}[s-1]), \quad (17)
 \end{aligned}$$

The KF estimation error, for  $s \neq 1$ , given by

$$\varphi_{jji}[s] = \mathbb{V}\{\hat{\mathbf{h}}_{jji}[s] - \hat{\mathbf{h}}_{jji}[s-1]\}, \quad (18)$$

is reduced to the estimation of a new channel vector at the  $s^{\text{th}}$  subcarriers. Thus, the current estimation becomes the previous estimation, i.e.,  $\hat{\mathbf{h}}_{jji}[s] \rightarrow \hat{\mathbf{h}}_{jji}[s-1]$ , and the channel variance is updated by

$$\sigma_{\hat{\mathbf{h}}_{jji}}[s] = (1 - \kappa_{jji}[s] x_{jji}[s]) \sigma_{\hat{\mathbf{h}}_{jji}}[s-1] + \varphi_{jji}[s]. \quad (19)$$

With the estimated channel variance,  $\kappa_{jji}[s]$  is updated till the channel at subcarrier  $S$  is estimated. However, the KF estimation should only be used with the MR receiver and with the proposed pilot mapping strategy. The reason is that it is necessary to reduce the interference effect on the received signal to perform KF estimation. Otherwise, the Kalman gain adjusts to the interference gain rather than the gain of the  $i^{\text{th}}$  UE channel.

## 4 Results and discussions

To test the performance of the proposed methodology in terms of the achievable SE for the UL and DL communications, we performed

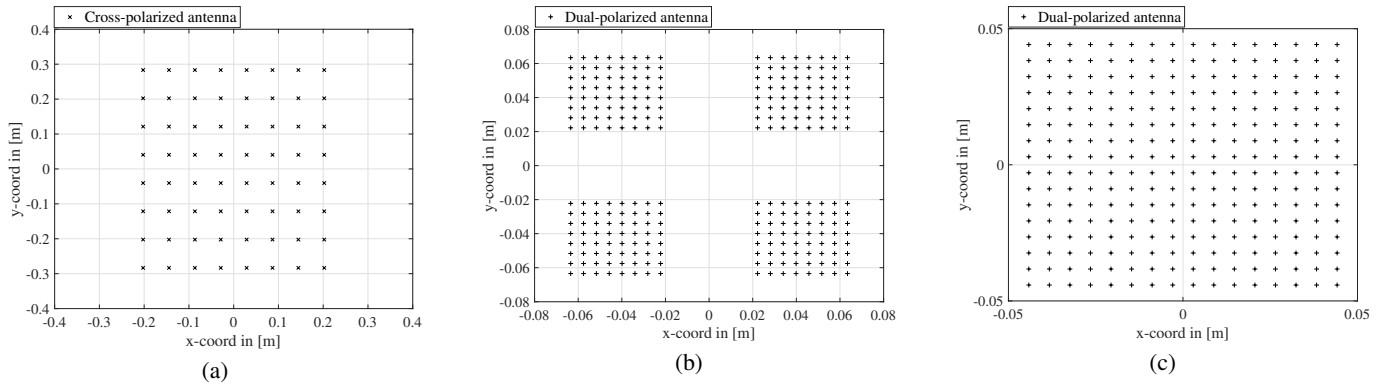


**Fig. 5:** Antenna arrays at the massive MIMO BS. (a) Fully-digital. (b) Partially-connected hybrid structure. (c) Fully-connected hybrid structure mmWave.

**Table 2** Hybrid beamforming simulation parameters

Parameter	Value
Channel model	mmMagic NLoS
UE array configuration	dual-antenna UEs
Cell radius	200 m
Carrier frequency	28 GHz
Carrier type	CP-OFDM (120 kHz of subcarrier spacing)
Carrier bandwidth	100 MHz
NR data slot	12 subcarriers per PRB, 14 OFDM symbols per slot / subframe, 66 PRBs
Occupied subcarriers	792 subcarriers per OFDM symbol
Channel estimation	LS, KF
Combining processing	MR, MMSE
<b>Partially-connected BS antenna properties</b>	
Number of antenna panels	4
Number of antenna elements per panel	$8 \times 8$ array with dual polarization (64T64R per polarization, $M = 512$ )
Element separation distance	$0.5 \lambda$
Number of RF chains / beams	8
Peak beam gain (dBi)	24
<b>Fully-connected BS antenna properties</b>	
Number of antenna panels	1
Number of antenna elements per panel	$16 \times 16$ array with dual polarization (256T256R per polarization, $M = 512$ )
Element separation distance	$0.5 \lambda$
Number of RF chains / beams	8
Peak beam gain (dBi)	27

extensive simulations based on the 5G NR Release 15 specifications [9]. Table 1 presents the parameters for the sub6-GHz band, where we assumed fully digital beamforming, whereas Table 2 presents the parameters for the mmWave band, for partially and fully-connected hybrid structures, according to [19, 23]. We assume hybrid beamforming for the mmWave band is only available at the BS, whereas for the UEs, only digital beamforming is considered.

With the parameters of Table 1 we set the fully-digital beamforming antenna array, according to the 3GPP 3D MIMO non-line-of-sight (NLoS) channel model for urban macrocell scenarios [24]. With the parameters of Table 2, we set the hybrid beamforming antenna array for partially- and fully-connected hybrid structures, according to the mmMagic channel model in [25]. In Fig. 5, we present the simulated antenna arrays, generated with the quasi-deterministic radio channel generator (QuaDRiGa) introduced in [23].

The array in Fig. 5(a) consists of 64 cross-polarized antennas, where each antenna is connected to a dedicated RF chain. Fig. 5(b) shows the partially connected hybrid array, which is divided into four panels. Each panel consists of  $8 \times 8$  dual-polarized antennas, where there is available one RF chain per polarization. Finally, Fig. 5(c) shows the fully connected hybrid array that consists of a single panel of  $16 \times 16$  dual-polarized antennas. Each polarized

array is connected to four RF chains. Both hybrid structures, fully- and partially-connected, consist of 512 antennas, where 256 antennas have vertical polarization, whereas the other 256 antennas have horizontal polarization. Hence, there are available eight RF chains for both structures.

The simulated sub6-GHz and mmWave multiuser multicell scenarios are presented in Fig. 6. Using  $L = 2$  cells, each cell consist of a fixed position BS and  $K = 2$  UEs. The positions of the UEs were configured to coincide with the border between the two cells. In Fig. 6, the BSs are represented with crosses, whereas the UEs are represented with triangles. BS1, UE1,1, and UE2,1 conform the cell 1, whereas BS2, UE1,2, and UE2,2 conform the cell 2. For the sub6-GHz band in Fig. 6(a), the radius of each cell is 500 m. The position of the devices for the sub6-GHz scenario is presented in Table 3.

The mmWave scenario in Fig. 6(b) is similar to that presented in Fig. 6(a), with  $L = 2$  and  $K = 2$  UEs per cell. However, in this case, the cell radius was set to 200 meters according to [8]. So, the position of the devices in the mmWave scenario is different than that in the sub6-GHz scenario. Table 4 presents the position of the devices in the mmWave scenario.

For the sub6GHz and mmWave scenarios, the position of the UEs starts from the border between the two cells. However, these positions change over one meter of mobility in random directions. For

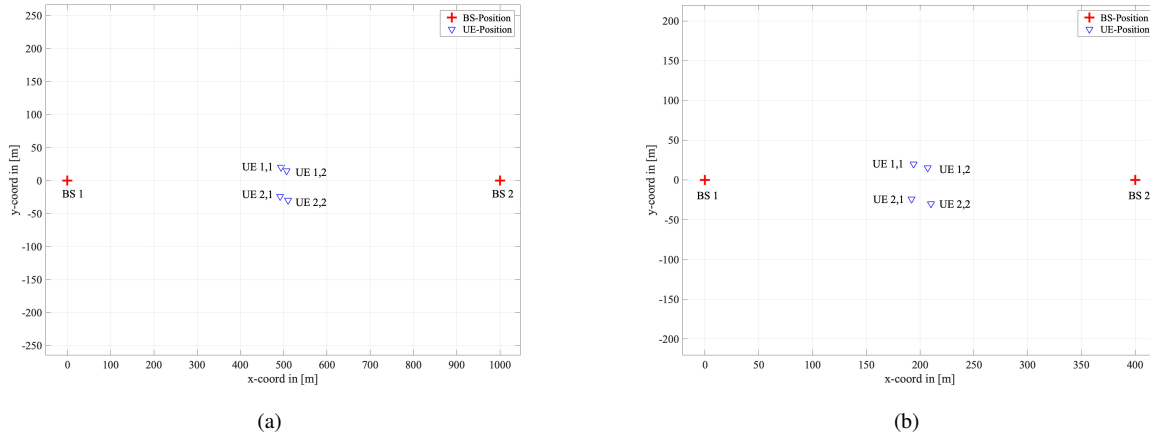


**Fig. 6:** Simulated multi-user multi-cell massive MIMO scenario. (a) Sub6-GHz scenario. (b) MmWave scenario

**Table 3** BSs and UEs positions in Cartesian coordinates for the sub6-GHz band scenario

Device	Initial position in meters		
	x	y	z
BS1 (fixed position)	0	0	20
UE1,1	494	20	1.5
UE2,1	492	-24	1.5
BS2 (fixed position)	1000	0	20
UE1,2	507	15	1.5
UE2,2	510	-30	1.5

this, we generated 2000 channel samples per meter for each UE in both scenarios.

For both scenarios, we set orthogonal pilots between UE1,1 and UE2,1, and we reused the same pilot sequence configured in UE1,1 and UE2,1 for UE1,2 and UE2,2. This way, we generated coherent interference as in [6]. Thus the frequency reuse factor for the cellular system is  $f = 1$ , which provokes pilot contamination. Non-coherent interference is present with the spatial multiplexing of multiple UEs that use orthogonal pilot sequences.

For fairness, we set the same total power and modulation scheme for every UE in the configured cells. We chose the 64-quadrature amplitude modulation (64-QAM) scheme for all the UEs, and signal-to-noise ratio is defined as  $\text{SNR} = \frac{\rho_{ji}}{\sigma_{jr}^2}$ . Furthermore, all the reported results were averaged over 2000 random channel realizations [13, 26].

Finally, to report the results, we compared the MR and MMSE receivers with and without the application of the pilot mapping described in Section 3. With regular pilot mapping, the one specified in the 5G NR Release 15 specifications, we used the LS estimation for all the receivers. However, with the application of the proposed pilot mapping, we used the KF estimation only for the MR receiver, since for MMSE processing, KF estimation is not suitable. With regular pilot mapping, the application of KF for the MR receiver is not suitable either since this estimator adjusts its gain to that of the interference, resulting in SE loss according to [22]. The improved MR and MMSE receivers are those with which we only used the proposed pilot mapping to reduce the effect of non-coherent interference (intra-cell interference). The configuration of the different MIMO techniques is summarized in Table 5.

#### 4.1 Sub6-GHz Spectral Efficiency

For the scenario of Fig. 6a, we present the sum SE of MIMO combining performed at the BSs in the UL communication in Fig. 7.

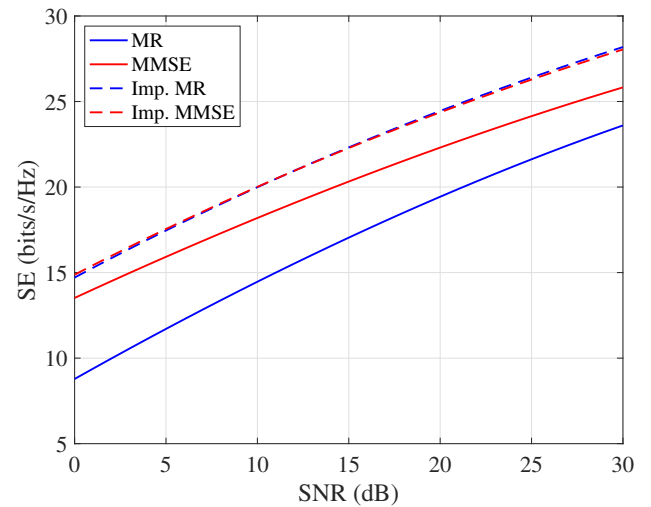


**Fig. 7:** Sub6-GHz UL sum SE of the MR and MMSE receivers with and without the proposed pilot training.

In Fig. 7, the achievable SE of the MR and MMSE receivers with regular pilot mapping is different. In this case, the MMSE receiver presents higher SE than the MR method, since the former is capable of partially removing the effects of coherent interference. The improved MR and MMSE receivers present similar SE, which is higher than that achieved with regular pilot mapping. Since the improved MR receiver employs the KF estimation, the achievable SE is comparable to that of the improved MMSE receiver with LS estimation.

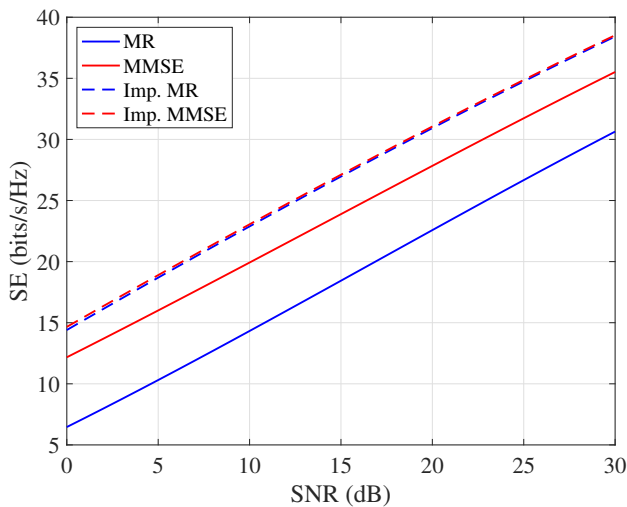
In Fig. 8, we present the sum SE results for MIMO combining processing performed at the UEs in the DL communication. In this case, the MIMO precoding vector processed by the BS in the UL is applied for DL transmission.

**Table 4** BSs and UEs positions in Cartesian coordinates for the mmWave band scenario

Device	Initial position in meters		
	x	y	z
BS1 (fixed position)	0	0	10
UE1,1	194	20	1.5
UE2,1	192	-24	1.5
BS2 (fixed position)	400	0	10
UE1,2	207	15	1.5
UE2,2	210	-30	1.5

**Table 5** MIMO processing settings

MIMO receiver	Estimator	Pilot mapping
MR	LS	Regular
MMSE	LS	Regular
Imp. MR	KF	New
Imp. MMSE	LS	New

**Fig. 8:** Sub6-GHz DL sum SE of the MR and MMSE receivers with and without the proposed pilot training.

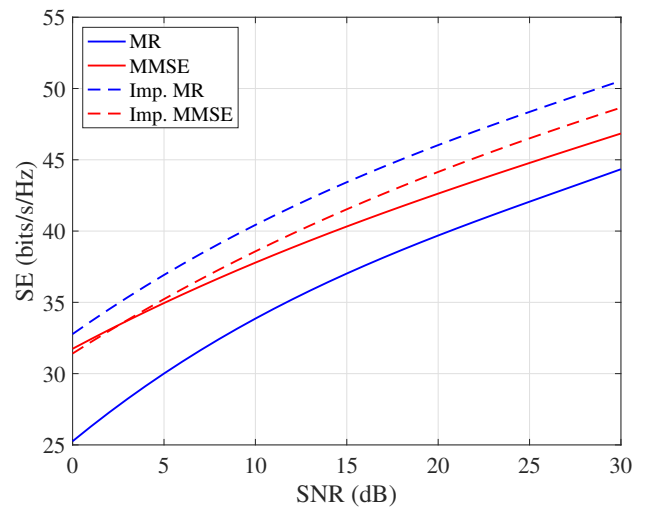
The results in Fig. 8 show that MR precoding applied with regular pilot mapping presents the smallest SE. However, when the new pilot mapping is used to find the precoding vector, the improved MR receiver presents a SE close to that of the MMSE receiver. Since the precoding is applied for the DL communications, the improved MR and MMSE receivers show similar results, which reveals that the effects of coherent and noncoherent interference are attenuated with the MIMO precoding processing performed at the BSs.

#### 4.2 MmWave Spectral Efficiency

For the mmWave scenario, it was necessary to perform MIMO combining and precoding on the received signal in BB, so the RF combining matrix was filtered as in (15) before the channel estimation process of the intended user described in Section 3.2. For the mmWave scenario (shown in Fig. 6b), Fig. 9 shows the sum SE results for MIMO combining processing performed with partially connected hybrid beamforming during the UL communication.

The results in Fig. 9 are similar to those for the sub6-GHz scenario in Fig. 7. However, the improved MR receiver presents higher SE than the improved MMSE method. In this case, the KF estimation helps the MR receiver to remove the effects of noise in the channel estimation process, therefore achieving higher SE.

Fig. 10 presents the SE results for MIMO combining processing performed at the UEs when MIMO precoding is performed with partially connected beamforming for the DL communication.

**Fig. 9:** Partially connected mmWave UL sum SE of the MR and MMSE receivers with and without the proposed pilot training.

As in the case of the DL results for the sub6-GHz scenario, Fig. 10 shows the improved MR, and MMSE receivers present similar results since MIMO precoding was used to transmit the signal from the BSs to the UEs.

In Fig. 11 we present the UL sum SE results achieved with a fully connected hybrid beamforming structure.

As it was expected, higher SE is achieved with the fully connected structure for the compared receivers. In this case, the SE of the improved MR receiver is significantly higher than that of the partially connected structure. Finally, we present the results for the fully connected hybrid beamforming structure for the DL communication.

Fig. 12 shows the SE results obtained with the fully connected structure, which are similar to those obtained with a partially-connected structure in Fig. 10.

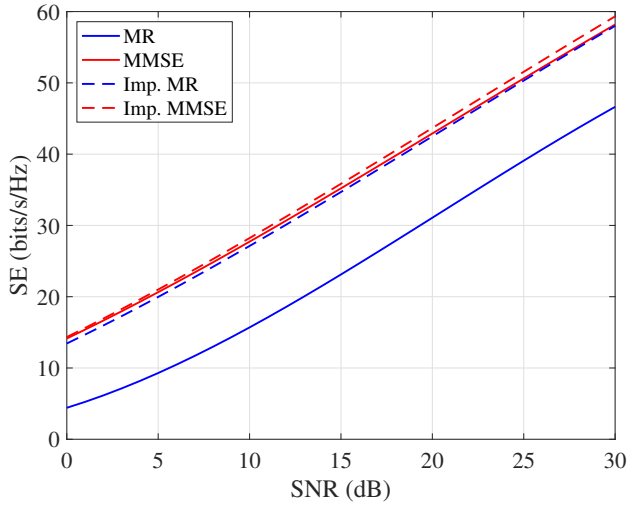
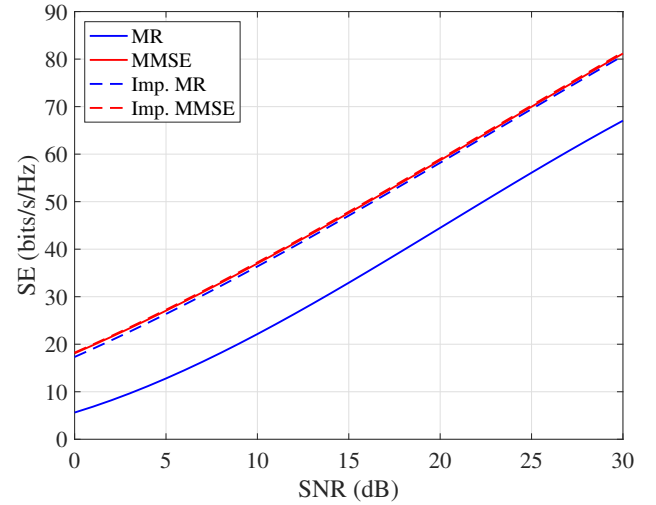
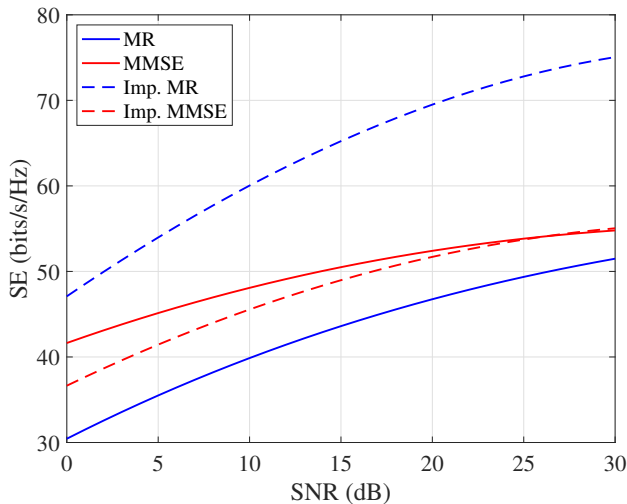
#### 4.3 Performance and complexity comparison

To run the simulations and get the results, we deliberately set the positions of the UEs in the border between the two configured cells. This way, the coherent and noncoherent interference power is sufficiently high to test the proposed methodology described in Section 3.

The SE of the improved MR receiver is similar to that of the improved MMSE receiver in the sub6-GHz band. However, in the mmWave band, the SE of the former is higher, especially for the fully connected hybrid structure, with which the SE is significantly higher. The more antennas at the BS, as is the case with a fully connected

**Table 6** Floating-point operations per UE of the different MIMO receivers

Method	Combining vector operations	Channel estimation
MR	$4KN_r - 1$	$KN_r^2$
MMSE	$N_r^3 + N_r^2(5K/2 + 2) + N_r(K + 1/2)$	$KN_r$

**Fig. 10:** Partially-connected mmWave DL sum SE of the MR and MMSE receivers with and without the proposed pilot training.**Fig. 12:** Fully-connected mmWave DL sum SE of the MR and MMSE receivers with and without the proposed pilot training.**Fig. 11:** Fully-connected mmWave UL sum SE of the MR and MMSE receivers with and without the proposed pilot training.

hybrid structure, the higher is the performance of the KF to remove the noise effects at the receiver. Since mmWave signals present high path loss, the effects of noise at mmWave frequencies are more significant than at lower frequencies. For this reason, the improved MR method shows higher SE than the MMSE receiver at mmWave frequencies since the former employs the KF algorithm, a technique capable of attenuating the effects of noise in the channel estimation process.

On the other hand, for DL transmission, the MIMO precoding performed with the proposed pilot mapping helps to mitigate the effects of coherent and noncoherent interference. In this case, we can expect that with the improved MR receiver, the UEs can achieve high SE with low computational complexity, avoiding resorting to more complex techniques such as the M-MMSE receiver.

Finally, Table 6 summarizes the floating-point operations required for MIMO combining processing at each BS. LS estimation is

assumed for the MMSE receiver, whereas for MR, KF estimation was used [27].

Based on the data of Table 6, the MR receiver requires much fewer operations than the MMSE receiver. Thus, the application of the proposed pilot mapping strategy and KF estimation at the MR receiver results in an SE comparable to that of the MMSE receiver with much fewer complex operations.

## 5 Conclusion

In this work, a novel method to perform channel estimation and reduce the interference effects present in multi-user multi-cell massive MIMO systems operating at 2.5 GHz and 28 GHz frequencies is analyzed. Coherent and noncoherent interference effects are attenuated through the use of a new pilot mapping strategy that allows us to reduce the interference effects provoked by users in the same cell as well as the user of interest and users in neighbor cells.

For operation frequencies below 6 GHz, MR processing with KF channel estimation and the proposed pilot mapping strategy, achieves similar performance as the MMSE receiver, requiring much fewer floating-point operations for MIMO processing. Furthermore, for mmWave frequencies, the improved MR processing results in higher SE than that achieved with the improved MMSE receiver, due to the effectiveness of the KF estimation to remove the effects of noise in signals with high path loss.

A UE can be subject to high coherent and noncoherent interference in the UL but not in the DL since the BS performs MIMO precoding for the latter. With the proposed pilot mapping strategy, the MIMO precoding processing used for DL transmission significantly reduces the interference for the spatially multiplexed UEs.

For the UEs, the advantage of MIMO precoding performed at the BS for DL transmission allows us to use the improved MR receiver and achieve a SE comparable to that of the MMSE receiver, with significantly lower computational complexity. This is useful for MIMO processing at the UE side.

## 6 Acknowledgments

This work was supported by the SEP-CONACyT Research Project 255387, the School of Engineering and Sciences, and the Telecommunications Research Focus Group at Tecnológico de Monterrey.

## 7 References

- 1 T. L. Marzetta, "Massive MIMO: An Introduction," *Bell Labs Technical Journal*, vol. 20, pp. 11–22, 2015.
- 2 Z. Chen and E. Björnson, "Channel hardening and favorable propagation in cell-free massive MIMO with stochastic geometry," *IEEE Transactions on Communications*, vol. 66, no. 11, pp. 5205–5219, 2018.
- 3 T. L. Marzetta, E. G. Larsson, H. Yang, and H. Q. Ngo, *Fundamentals of Massive MIMO*. Cambridge University Press, 2016.
- 4 E. Björnson, J. Hoydis, and L. Sanguinetti, "Massive MIMO has unlimited capacity," *IEEE Transactions on Wireless Communications*, vol. 17, no. 1, pp. 574–590, 2017.
- 5 J. Beiranvand and H. Meghdadi, "Analytical performance evaluation of mrc receivers in massive mimo systems," *IEEE Access*, vol. 6, pp. 53 226–53 234, 2018.
- 6 L. Sanguinetti, E. Björnson, and J. Hoydis, "Towards massive MIMO 2.0: Understanding spatial correlation, interference suppression, and pilot contamination," *IEEE Transactions on Communications*, pp. 1–1, 2019.
- 7 I. Boukhedimi, A. Kammoun, and M. Alouini, "Multi-cell MMSE combining over correlated rician channels in massive MIMO systems," *IEEE Wireless Communications Letters*, vol. 9, no. 1, pp. 12–16, 2020.
- 8 M. R. Akdeniz, Y. Liu, M. K. Samimi, S. Sun, S. Rangan, T. S. Rappaport, and E. Erkip, "Millimeter wave channel modeling and cellular capacity evaluation," *IEEE Journal on Selected Areas in Communications*, vol. 32, no. 6, pp. 1164–1179, 2014.
- 9 E. Dahlman, S. Parkvall, and J. Skold, *5G NR: The Next Generation Wireless Access Technology*. Academic Press, 2018.
- 10 J. Zhang, X. Yu, and K. B. Letaief, "Hybrid beamforming for 5G and beyond millimeter-wave systems: A holistic view," *IEEE Open Journal of the Communications Society*, vol. 1, pp. 77–91, 2020.
- 11 S. Han, I. Chih-Lin, Z. Xu, and C. Rowell, "Large-scale antenna systems with hybrid analog and digital beamforming for millimeter wave 5G," *IEEE Communications Magazine*, vol. 53, no. 1, pp. 186–194, 2015.
- 12 I. Ahmed, H. Khammari, A. Shahid, A. Musa, K. S. Kim, E. De Poorter, and I. Moerman, "A survey on hybrid beamforming techniques in 5G: Architecture and system model perspectives," *IEEE Communications Surveys Tutorials*, vol. 20, no. 4, pp. 3060–3097, 2018.
- 13 O. El Ayach, S. Rajagopal, S. Abu-Surra, Z. Pi, and R. W. Heath, "Spatially sparse precoding in millimeter wave MIMO systems," *IEEE transactions on wireless communications*, vol. 13, no. 3, pp. 1499–1513, 2014.
- 14 T. L. Marzetta, "Noncooperative cellular wireless with unlimited numbers of base station antennas," *IEEE Transactions on Wireless Communications*, vol. 9, no. 11, pp. 3590–3600, 2010.
- 15 A. Khansefid and H. Minn, "Achievable downlink rates of MRC and ZF precoders in massive MIMO with uplink and downlink pilot contamination," *IEEE Transactions on Communications*, vol. 63, no. 12, pp. 4849–4864, 2015.
- 16 A. F. Molisch, V. V. Ratnam, S. Han, Z. Li, S. L. H. Nguyen, L. Li, and K. Haneda, "Hybrid beamforming for massive MIMO: A survey," *IEEE Communications Magazine*, vol. 55, no. 9, pp. 134–141, 2017.
- 17 H. Li, T. Q. Wang, X. Huang, J. A. Zhang, and Y. J. Guo, "Low-complexity multiuser receiver for massive hybrid array mmWave communications," *IEEE Transactions on Communications*, vol. 67, no. 5, pp. 3512–3524, 2019.
- 18 Z. Wang, M. Li, Q. Liu, and A. L. Swindlehurst, "Hybrid precoder and combiner design with low-resolution phase shifters in mmWave MIMO systems," *IEEE Journal of Selected Topics in Signal Processing*, vol. 12, no. 2, pp. 256–269, 2018.
- 19 A. Zaidi, F. Athley, J. Medbo, U. Gustavsson, G. Durisi, and X. Chen, *5G Physical Layer: Principles, Models and Technology Components*. Academic Press, 2018.
- 20 S. H. Ting, K. Sakaguchi, and K. Araki, "A Markov-Kronecker model for analysis of closed-loop MIMO systems," *IEEE Communications Letters*, vol. 10, no. 8, pp. 617–619, 2006.
- 21 J. Rodríguez-Fernández, N. González-Prelcic, K. Venugopal, and R. W. Heath, "Frequency-domain compressive channel estimation for frequency-selective hybrid millimeter wave mimo systems," *IEEE Transactions on Wireless Communications*, vol. 17, no. 5, pp. 2946–2960, 2018.
- 22 D. F. Carrera, C. Vargas-Rosales, L. Azpilicueta, and J. A. Galaviz-Aguilar, "Comparative study of channel estimators for massive MIMO 5G NR systems," *IET Communications*, vol. 14, pp. 1175–1184(9), April 2020. [Online]. Available: <https://digital-library.theiet.org/content/journals/10.1049/iet-com.2019.0973>
- 23 S. Jaeckel, L. Raschkowski, K. Börner, L. Thiele, F. Burkhardt, and E. Eberlein, "Quasi deterministic radio channel generator user manual and documentation," *Fraunhofer Heinrich Hertz Institute, Tech. Rep. v1*, pp. 4–1, 2016.
- 24 B. Mondal, T. A. Thomas, E. Visotsky, F. W. Vook, A. Ghosh, Y. Nam, Y. Li, J. Zhang, M. Zhang, Q. Luo, Y. Kakishima, and K. Kitao, "3D channel model in 3GPP," *IEEE Communications Magazine*, vol. 53, no. 3, pp. 16–23, 2015.
- 25 M. Tercero, P. von Wrycza, A. Amah, J. Widmer, M. Fresia, V. Frascolla, J. Lorca, T. Svensson, M. Hamon, S. D. Roblot, A. Vijay, M. Peter, V. Sgardoni, M. Hunukumbure, J. Luo, and N. Vucic, "5G systems: The mmMAGIC project perspective on use cases and challenges between 6–100 GHz," in *2016 IEEE Wireless Communications and Networking Conference Workshops (WCNCW)*, 2016, pp. 200–205.
- 26 V. Bota and M. Varga, "On the BER and spectral efficiency performances of coded QAM configurations that map non-coded bits," in *2016 International Conference*

on Communications (COMM), June 2016, pp. 223–228.  
27 R. Hunger, *Floating Point Operations in Matrix-Vector Calculus*. Munich University of Technology, Inst. for Circuit Theory and Signal Processing, 2005.